Graphical Abstract

Technology Neutral Quantification of automatic frequency reserve contribution to frequency stability in power systems using Frequency Domain System Identification

Karl-Fredrik Kylesten, Robert Eriksson

1.

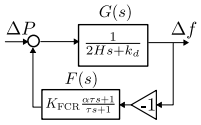

In a simplified case, the closed loop transfer functio $\Delta P \to \Delta f$ can be writtenon on SOPZ form

$$T(s) = R_{\text{tot}} \frac{\tau_z s + 1}{s^2 + 2\zeta\omega_0 s + \omega_0^2}$$

2.

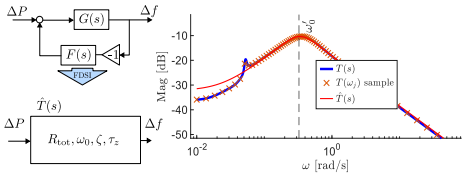

With FDSI we use curve fitting in the frequency domain to gen a SOPZ approximation $\hat{T}(s)$(red) from a more complex model $T(s)$ (blue).

3.

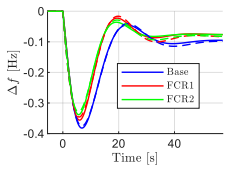

The SOPZ model $\hat{T}(s)$ (dashed lines) gave simmilar step response as original model $T(s)$(solid lines).

4.

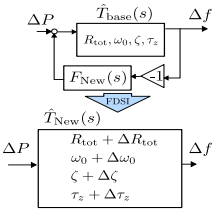

We can use this to:

- Quantify frequency dynamics
- Quantify contribution of frequency reserves

Highlights

Technology Neutral Quantification of automatic frequency reserve contribution to frequency stability in power systems using Frequency Domain System Identification

Karl-Fredrik Kylesten, Robert Eriksson

- A technology-neutral method is proposed for quantifying frequency dynamics using frequency-domain system identification (FDSI).
- A reduced second-order-plus-zero (SOPZ) model accurately captures the dominant behaviour of complex closed-loop frequency control systems.
- The four SOPZ parameters provide interpretable metrics that enable consistent comparison of diverse reserve technologies.
- A hydropower case study demonstrates the method's ability to quantify reserve contributions and link system dynamics to classical performance indicators.

Technology Neutral Quantification of automatic frequency reserve contribution to frequency stability in power systems using Frequency Domain System Identification

Karl-Fredrik Kylesten[a], Robert Eriksson[a]

[a]*Department of Electrical Enginering Uppsala university, Ångströmlaboratoriet, Lägerhyddsvägen 1, Uppsala, 752 37, Sweden*

Abstract

This study proposes a technology-neutral method for quantifying power system frequency dynamics and evaluating the contribution of ancillary services to frequency control. The approach applies frequency-domain system identification to the closed-loop interaction between the grid and primary reserves, yielding a reduced second-order-plus-zero transfer function with four parameters. The SOPZ model reproduces the dominant behaviour of the system. These parameters provide interpretable metrics linking control concepts to system properties and enable the comparison of reserve technologies.

Performance indicators, including the frequency nadir and phase margin, were derived from the reduced model. A case study based on a hydropower plant showed that the method captures the differences between governor reserves and quantifies their contributions to the system response. Although the RoCoF and equivalent inertia were less accurately estimated, the method

*Corresponding author

Email address: karl-fredrik.kylesten@angstrom.uu.se (Karl-Fredrik Kylesten)

provides a framework for analysing reserve performance. This establishes a foundation for evaluating frequency control services in low-inertia-power systems.
Keywords: Power system, Frequency stability, Ancillary services, Primary frequency control, Control theory, Linear model

1. Introduction

The stability of the power system frequency is essential for secure and reliable grid operation. Frequency deviations outside acceptable limits can cause the disconnection of generators or loads, potentially leading to cascading failures [1]. Because frequency directly reflects the balance between the generated and consumed active power through the swing equation, maintaining this balance is a fundamental task for system operators [2]. Load Frequency Control (LFC) uses active power reserves, such as power plants that can adjust production, to counter power imbalances and maintain the frequency at its nominal value. One of the most common reserves is the Frequency Containment Reserve (FCR), also known as the primary reserve, which is automatically activated based on local frequency measurements. FCR typically operates through the governor-based droop control of synchronous generators (SGs). SGs also contribute to stability by storing rotational energy, thereby adding inertia to the system and helping to limit the Rate of Change of Frequency (RoCoF) [2].

As the power system landscape continues to evolve, maintaining frequency stability is becoming increasingly challenging. The dynamic properties of the grid fundamentally change as the penetration of inverter-based renew-

able energy sources (IRES) increases. The implications of declining inertia for frequency stability have been widely studied [3], and recent studies have explored how ancillary services can compensate for low-inertia conditions. However, much of this work still implicitly assumes ancillary service definitions and performance metrics that are rooted in synchronous-machine-based system dynamics. In these systems, the grid relies heavily on inverter-based resources, including renewable generation, energy storage, and HVDC links, not only for energy production but also for frequency support.

The properties of IRES are different from those of traditional resources. On one hand, inverters can operate faster than governor-based turbines, and new resources have the potential to support the grid with fast responses. However, these resources may be limited by the available power from the weather or the state of charge in battery storage systems. The requirements and compensation schemes for different ancillary service products are usually designed for traditional reserves, making it difficult for IRES to contribute [4, 5]. Solutions include new ancillary services that better utilise the speed of inverters, compensation models based on performance that could reward speed, and redesigned requirements for participating in the market [6, 7]. Despite these proposals, no widely adopted framework exists for quantitatively linking system-level frequency needs to the measurable dynamic properties of aggregated resources.

To evaluate new ancillary services and performance-based compensation models, it is crucial to understand both the needs of the power system and the contribution of individual reserves to the overall frequency dynamics. This requires metrics that describe the system dynamics independently of the un-

derlying technology used to deliver the frequency support. To include a broad range of technologies, the metrics used for evaluation must be technology-neutral. Examples of system-level performance indicators include metrics derived from the frequency response following a load disturbance, such as the maximum RoCoF, frequency nadir, and steady-state frequency deviation (SSFD) [2]. For stability assessment, classical control metrics such as the phase and gain margins are commonly used [8].

However, these indicators are typically evaluated individually and do not provide a compact representation of the underlying closed-loop frequency dynamics of the system. This study addresses this gap by developing a method based on the Frequency Domain System Identification (FDSI) approach. The method characterises the frequency dynamics of a closed-loop (CL) system using four parameters that describe its essential dynamic behaviour. These parameters can be analytically related to conventional performance indicators, including the maximum RoCoF, frequency nadir, and phase and gain margins, thereby providing an interpretable connection between classical control theory and system-level frequency performance.

Finally, to demonstrate the applicability of the proposed approach, the method was tested in a case study using a reference hydropower plant model. The results show that the reduced-order model obtained through the FDSI accurately captures the frequency dynamics of the system and enables a meaningful quantification of each reserve's contribution.

2. Motivation for simplified model

We represent the aggregate frequency dynamics using the classical swing equation with load damping. Under the Single Machine Equivalent (SME) assumption, the system's inertial response is captured by the aggregated inertia constant H, and the frequency-sensitive load and generator damping are represented by k_d. Linearising around an operating point yields the familiar first-order relation between the power imbalance $\Delta P(s)$ and the frequency deviation $\Delta f(s)$,

$$G(s) = \frac{\Delta f(s)}{\Delta P(s)} = \frac{1}{2Hs + k_d}, \tag{1}$$

which serves as a grid model for load frequency dynamics without frequency control.

To analyse the frequency containment control, we consider a controller $F(s)$ acting on the measured frequency deviations. The open-loop transfer function is

$$G_O(s) = G(s)F(s), \tag{2}$$

from which the sensitivity function

$$S(s) = \frac{1}{1 + G(s)F(s)} \tag{3}$$

can be derived. We also define

$$T(s) = G(s)S(s) = \frac{G(s)}{1 + G(s)F(s)}, \tag{4}$$

which describes how load disturbances propagate to frequency under closed-loop control and forms the basis for evaluating the dynamic contribution of different reserve technologies.

For the frequency reserve, we considered an idealised plant model without a phase shift or time delay as a starting point, in which the output power always followed the input reference in proportion. Under this assumption, we model the FCR plant simply as

$$F_{\mathrm{FCR}}(s) = K_{\mathrm{FCR}}, \tag{5}$$

where K_{FCR} represents the plant gain. To avoid future confusion regarding the terms "droop" and "droop-gain" we will clarify that we will adopt the convention used in the literature, such as [9] and [8]. We can define the droop coefficient or just droop as

$$R = \frac{\Delta f}{\Delta P} = (K_{\mathrm{FCR}})^{-1}, \tag{6}$$

which expresses how much the frequency is allowed to deviate (Δf for a certain change in the generating power, ΔP). For example, if we put the expressions from Eq. (5) into Eq. (4) reveals that An ideal FCR controller increases the effective damping of the system to $k_d + K_{FCR}$. In this study, we will call

$$R_{\mathrm{tot}} = \frac{1}{R + k_d} \tag{7}$$

the total droop. The steady-state frequency deviation (SSFD)in the system is reduced to $\Delta P R_{\mathrm{tot}}$.

However, this idealised plant model is not realistic for practical applications. In reality, plant dynamics are governed by complex nonlinear behaviour. However, for small-signal analysis, a linear approximation can be employed, which is typically represented by transfer functions comprising gains, poles, and zeros. Inspired by [10], we want $T(s)$ to be of second order

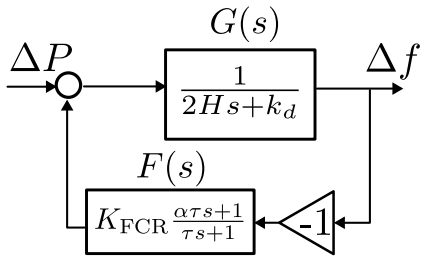

Figure 1: Base model used for the motivation of SOPZ model

to compute the step response analytically and use the term from classical control theory to describe the system. If $T(s)$ is second order, and $G(s)$ is of first order, then $F(s)$ must be of first order as well.

In [9], a transfer function with one pole and one zero was used to approximate the behaviour of various generator plant types, including hydroelectric, gas turbine, and wind power plants. Based on this insight, we introduce the following general model.

$$F_{\mathrm{Plant}}(s) = \frac{\tau\alpha s + 1}{\tau s + 1}, \tag{8}$$

where τ is the time constant characterising the rise time of the plant's step response, and α is a shaping factor that modulates the plant's response.

2.1. Closed-loop model of FCR and Grid, Second order plus zero

To analyse the CL system of a power system with LFC, we consider a scenario in which the grid, represented by $G(s)$ in Eq. (1) is combined with the plant model in Eq. 8 to describe the fynamics o our ancillary servise. These expressions can now be used in Eq. (4) to examine the CL system dynamics under more realistic assumptions. With this FCR plant, we get the closed loop system like in Fig. 1 and $T(s)$ becomes

$$T(s) = \frac{\tau s + 1}{(2Hs + k_d)(\tau s + 1) + K_{FCR}(\alpha\tau s + 1) + k_d} \tag{9}$$

We can see that $T(s)$ is a second-order transfer function with two poles and one zero or lead factor. In Eq. (9), $T(s)$ is expressed in the base (H, k_d, τ, α and K_{FCR}), wich corresponds to the equivalent system, However, $T(s)$ can also be expressend in another base, so that we get $T(s)$ written on a form more common in control theory, and we will call this transfer function second-order plus zeros (SOPZ):

$$T(s) = R_{\mathrm{tot}}\omega_0^2 \frac{\tau_z s + 1}{s^2 + 2\zeta\omega_0 s + \omega_0^2}. \tag{10}$$

The parameters in (10), referred to here as the SOPZ parameters, are the natural frequency ω_0, the damping coefficient ζ ($0 < \zeta < 1$ for under-damping and $\zeta > 1$ for over-damping), and the numerator time constant τ_z, which determines the zero of $T(s)$ and coincides with τ when a single reserve is considered. By expanding the denominator in Eq. (9), we can evaluate the SOPZ-parameters as

$$\omega_0\zeta = \frac{k_d\tau + K_{\mathrm{FCR}}\tau\alpha + 2H}{2H\tau} \tag{11}$$

$$\omega_0 = \sqrt{\frac{k_d + K_{\mathrm{FCR}}}{2H\tau}}, \tag{12}$$

and

$$\zeta = \frac{k_d\tau + K_{\mathrm{FCR}}\tau\alpha + 2H}{4H\tau} \Big/ \sqrt{\frac{k_d + K_{\mathrm{FCR}}}{2H\tau}}. \tag{13}$$

3. Frequency Domain System Identification

In this study, we suggest the use of Frequency Domain System Identification (FDSI) to quantify the properties of frequency dynamics.

In FDSI, we have a model $F(s)$, and a simplified model $\hat{F}(s,\theta)$ with parameters $\theta = \{\theta_1, \theta_2 \dots\}$, which we want to tune so that $\hat{F}(s,\theta)$ matches $F(s)$. The FDSI aims to identify the θ that minimize the error

$$\varepsilon(s) = \hat{F}(s,\theta) - F(s) \tag{14}$$

for all s. This is achieved by sampling a set of frequencies ω_i, assigning weights w_i, and formulating the cost function

$$V(\theta) = \sum_i w_i ||\hat{F}(j\omega_i,\theta) - F(j\omega_i)|| \tag{15}$$

Subsequently, an optimization algorithm is employed to determine the θ that minimizes $V(\theta)$. The sample density is most commonly logarithmic[11].

4. Frequency Domain System Identification as a Method for Quantifying System properties

To implement this method, as shown in Fig. 3, we need a model for our grid $G(s)$ and a model for the total of all our automatic frequency reserves $F(s)$, which we use to construct $T(s)$, see (4). We then use the FDSI to tune the parameters $R_{\text{tot}}, \omega_0, \zeta, \tau_z$ from the SOPZ transfer function, so that we obtain an estimation $\hat{T}(s)$. Matlab handles this process automatically with the built-in function *procest*, which also returns a fit-score

$$\text{fit}_{\%} = 100 \cdot \frac{\sum_i |\hat{T}(j\omega_i) - F(j\omega_i)|^2}{\sum_i |F(j\omega_i)|^2} \tag{16}$$

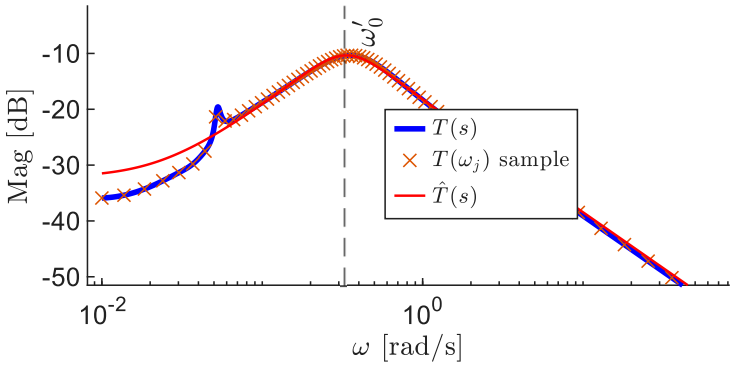

Figure 2: Example of FDSI. The density of sampled frequencies are closest around an estimation, ω_0'

0-100 % that tells us how well the the final $\hat{F}(s,\theta)$ matches the frequency response of $F(s)$. In system identification, an 80% fit score is considered a good fit[12]. The frequencies sampled ω_i for the FDSI were selected such that the sample density was higher for the range of frequencies that could be critical for the system. It was assumed that this frequency range was close to ω_0. Therefore, the FDSI was performed in two parts, as illustrated in figure 2. 1) An initial estimation of ω_0 was performed by estimating $\hat{T}(s)$ with 100 frequency samples logarithmically distributed between 10^{-2} and 10^{2} rad/s (2): Another 5000 frequencies were sampled in a such that the the sample density function was normally distributed over $\log(\omega)$ around $\log(\omega_0)$. That is, the density of the samples is proportional to $1 + a\exp\{(\log\omega_0 - \log\omega)^2/(2\sigma_\omega)\}$ where a and σ_ω are the shape parameters. Another $\hat{T}(s)$ was estimated using the new, increased sample size. With this estimation, we obtain our estimations of $R_{\text{tot}}, \omega_0, \zeta, \tau_z$. Together, these four metrics quantify the system performance and dynamics.

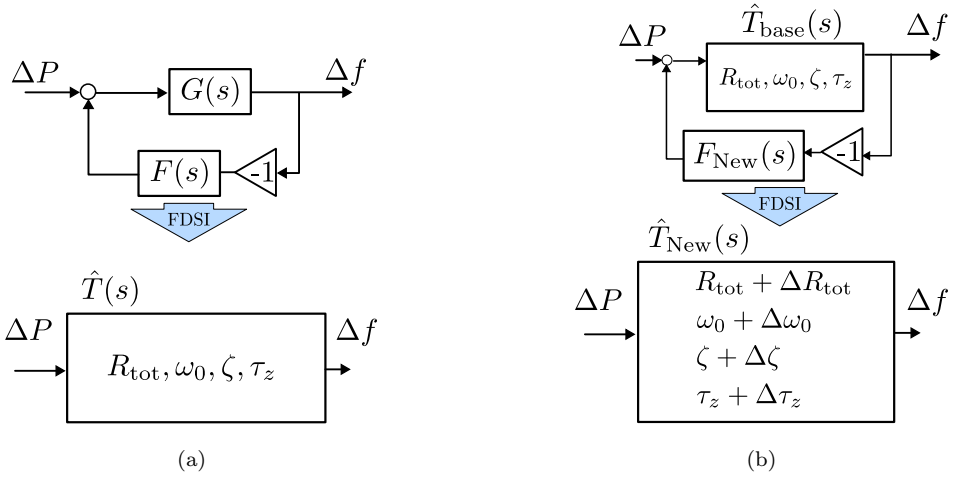

Figure 3: Illustration of usage for the method. (a): FDSI is used on a system with grid model $G(s)$ and reserve model $F(s)$ to fit the SOPZ model $\hat{T}(s)$. (b): FDSI is used to quantify the contribution of one additional reserve $F_{\text{New}}(s)$.

When we identify $T(s)$ with the FDSI, it is expressed in the standard form for the SOPZ transfer function with the parameters $(R_{\text{tot}}, \omega_0, \zeta, \tau_z)$. Representing $T(s)$ in standard form is useful for classical control theory, as ω_0 and ζ express oscillations and damping of $T(s)$.

In addition to quantifying the stability and performance of the system as a whole, the FDSI can also be implemented to estimate the contribution of a single additional reserve $F_{\text{New}}(s)$ that is to be implemented in a grid that already has other reserves. As illustrated in Fig. 3 (b), we have already used the FDSI and obtained an estimation $\hat{T}_{\text{base}}(s)$ that describes the base case of our system. We then introduce $F_{\text{New}}(s)$ and construct $T_{\text{New}}(s) = \hat{T}_{\text{base}}(s)/(1+\hat{T}_{\text{base}}(s)F_{\text{New}}(s))$. Then, we use the FDSI to obtain $\hat{T}_{\text{New}}(s)$, which will have the parameters $\theta + \Delta\theta$, where $\Delta\theta$ can be considered as a quantification of the contribution of $F_{\text{New}}(s)$. We can express the contribution of $F_{\text{New}}(s)$ either

with the base $(\Delta R_{\text{tot}}, \Delta\omega_0, \Delta\zeta, \Delta\tau_z)$ or the base $(\Delta R_{\text{eq}}, \Delta H_{\text{eq}}, \Delta\tau_z, \Delta\alpha_{\text{eq}})$

5. Relation to other common metrics

One benefit of reducing $T(s)$ to a second-order transfer function is that it becomes more manageable for analytical purposes. Typically, the performance, stability, and robustness metrics are assessed through simulations. However, if we obtain $(R_{\text{tot}}, \omega_0, \zeta, \tau_z)$ via FDSI, many different metrics can be readily derived depending on the focus of the study.

5.1. Step response metrics

As a metric for how well the CL system $T(s)$ can handle disturbances, we derive the frequency nadir (FN) Δf_{Max}. The FN depends on the disturbance we want to test, but a common choice is to let $\Delta P(s)$ be a step function that goes from 0 to dP at $t = 0$. We can then derive the step response $f(t)$ of $T(s)$ as

$$\Delta f(s) = \mathcal{L}^{-1}\left\{ dP R_{\text{tot}} \omega_0^2 \frac{\tau_z s + 1}{s^2 + 2\zeta\omega_0 s + \omega_0^2} \cdot \frac{1}{s} \right\}(t), \tag{17}$$

since $1/s$ is the transform of a unit step. The FN Δf_{Max} can be found as $\Delta f(t_{\text{nadir}})$ where t_{nadir} is the first t that satisfies $\text{RoCoF}(t_{\text{nadir}}) = 0$.

The solution for $\Delta f(t)$ varies depending on whether the system is overdamped or underdamped: For the underdamped case, we know that the poles are

$$p_{1,2} = \omega_0\zeta \pm j\omega_d \tag{18}$$

where

$$\omega_d = \omega_0\sqrt{1 - \zeta^2} \tag{19}$$

is the damped frequency, and taking the inverse transform in the under-damped case gives the solution

$$\Delta f_{\mathrm{UD}}(t) = dPR_{\mathrm{tot}} \left[1 - \exp\{-\zeta\omega_0 t\} \left(\cos\omega_d t + \frac{\zeta - \tau\omega_0}{\sqrt{1-\zeta^2}} \sin\omega_d t \right) \right] \quad (20)$$

An interesting property of $T(s)$ is that we can obtain an overshoot even in the over-damped case where $\zeta > 1$, owing to the effect of the zeros located at $z = -1/\tau_z$; therefore, we also need a solution for the over-damped case. We do the substitutions

$$\beta = \omega_0 \sqrt{\zeta^2 - 1} \quad (21)$$

and obtain the step response for the over-damped case

$$\Delta f_{\mathrm{OD}}(t) = dPR_{\mathrm{tot}} \left[1 + \exp\{-\omega_0\zeta\} \left(-\cosh\beta t + \frac{\tau_z\omega_0^2 - \zeta\omega_0}{\beta} \sinh\beta t \right) \right] \quad (22)$$

It can be shown that there will be an overshoot if

$$0 < \frac{\tau_z\omega_0^2\beta}{\omega_0\zeta(\tau_z\omega_0^2 - \zeta\omega_0) + \beta^2} < 1. \quad (23)$$

Then, the overshoot happens at

$$t_{\mathrm{nadir,OD}} = \frac{1}{\beta} \tanh^{-1} \left(\frac{\tau_z\omega_0^2\beta}{\omega_0\zeta(\tau_z\omega_0^2 - \zeta\omega_0) + \beta^2} \right) \quad (24)$$

Otherwise, when there is no overshoot, the FN is the same as the SSFD, that is

$$\Delta f_{\mathrm{Final}} = \lim_{s\to 0} dPR_{\mathrm{tot}}\omega_0^2 \frac{\tau_z s + 1}{s^2 + 2\zeta\omega_0 s + \omega_0^2} = dPR_{tot}. \quad (25)$$

From the step equation, we can also see that the maximum RoCoF, $\mathrm{RoCoF}_{\mathrm{max}}$, occurs immediately after the step response and is proportional to the inverse

of the inertia. The inertia is not measured directly with our method, but by using Eq. 11 - 13, we can obtain an equivalent inertia,

$$H_{\text{eq}} = \frac{1}{2\omega_0^2 R_{\text{tot}} \tau_z}, \tag{26}$$

describes the inertia that an equivalent system with the same SOPZ parameters would have if we assume the same structure as described in Fig. 1.

5.2. Analytical Phase and Gain margin

In a stable system, avoiding the singularity of the sensitivity function $S(s)$. According to the Nyquist stability criterion, the loop transfer function $G_0(j\omega)$ must not encircle the critical point -1. The phase margin (PM) and gain margin (GM) serve as quantitative indicators of the proximity of $G_0(j\omega)$ to the critical point. Notably, these margins are metrics of robustness rather than absolute stability tests: the PM denotes the extent of additional phase lag that can be tolerated at the gain crossover before the onset of instability, whereas the GM represents the extent of multiplicative gain increase that can be tolerated[11]. Thus, the SOPZ model can be applied not only for performance analysis but also for evaluating robustness.

The OL system can be expressed as

$$G_0(s) = \frac{1 + \tau\alpha s}{(2Hs + k_d)(1 + \tau s)} = \tau_z \omega_0^2 \frac{1 + s\,\frac{\tau_z\omega_0\zeta - 1}{\tau_z\omega_0}}{s\,(1 + s\tau_z)}. \tag{27}$$

Substituting $s = j\omega$ yields the magnitude is

$$|G_0(j\omega)| = \frac{\tau_z\omega_0^2}{\omega} \frac{\sqrt{1 + \omega^2 \left(\frac{\tau_z\omega_0\zeta - 1}{\tau_z\omega_0}\right)^2}}{\sqrt{1 + (\omega\tau_z)^2}}, \tag{28}$$

and the phase is

$$\angle G_0(j\omega) = \arctan\left(\omega\,\frac{\tau_z\omega_0\zeta - 1}{\tau_z\omega_0}\right) - \arctan(\omega\tau_z) - \frac{\pi}{2}. \tag{29}$$

The gain margin is obtained from the phase crossover frequency ω_{pc}, where $\angle G_0(j\omega) = \pm\pi$. Solving for this frequency gives

$$\omega_{pc} = \sqrt{\frac{\omega_0^2}{1 - \zeta\omega_0\tau_z}}. \tag{30}$$

The condition for a real solution of ω_{pc} is $\tau_z\omega_0\zeta < 1$. When a real solution exists, the gain margin is $\mathrm{GM} = 1/|G_0(j\omega_{pc})|$; otherwise, the Nyquist curve does not cross the real axis, and the gain margin is effectively infinite, making GM an uninformative robustness metric.

In contrast, the phase margin is determined from the gain crossover frequency ω_{gc} defined by $|G_0(j\omega_{gc})| = 1$. Introducing the substitution

$$C = 1 - \left(\tau_z\omega_0^2\frac{\tau_z\omega_0\zeta - 1}{\tau_z\omega_0}\right)^2, \tag{31}$$

one obtains

$$\omega_{gc}^2 = \frac{-C + \sqrt{C^2 + 4(\tau_z\omega_0^2)}}{2\tau_z}, \tag{32}$$

and the phase margin is then

$$\mathrm{PM} = \arctan\left(\omega_{gc}\frac{\tau_z\omega_0\zeta - 1}{\tau_z\omega_0}\right) - \arctan(\omega_{gc}\tau_z) + \frac{\pi}{2}. \tag{33}$$

It can be shown that for an underdamped system, PM is approximately proportional to ζ, which corresponds with the fact that the real part of the dominant poles is also proportional to ζ.

6. Case Study: Addition of Hydro Power FCR

In this section, we demonstrate how the proposed method can be applied to quantify the impact of introducing new reserves into the system. Hydropower was selected as the reference model because it has been well-studied and often serves as a benchmark in studies of frequency dynamics. First, we introduced a base with a single hydropower plant. Subsequently, additional hydropower plants will be introduced one at a time. Using the FDSI, we investigated how the properties of the system changed and evaluated these additional reserves.

6.1. The cases

The reference model in this case study is a linear model of a hydropower plant obtained from [2]. The model describes the dynamics of the position of the water gate and servo, as well as of the generator and penstock, and can be written as

$$F_{\text{Hydro}}(s) = \frac{T_R s + 1}{(1 + T_{g1}s)(1 + T_{g2}s)} \frac{1 - 2T_w}{1 + T_w s} \tag{34}$$

When the plant is automatically controlled with droop R, the parameters T_{g1} and $T_{g2}$are obtained as

$$T_{g1} = \frac{T_R T_G}{T_G + T_R(R + g_{st})} \tag{35}$$

and

$$T_{g2} = \frac{T_G + T_R(R + g_{st})}{R}. \tag{36}$$

Typical values for T_R and T_g are 2.5–7.5 and 0.2–0.4 s, respectively, and typical values for g_{tr} are 0.2-1.0. [2].

In the base case, the system consists of a grid model $G(s)$ with $H = 4.5$ and $k_d = 0.01$ and a power base $S_b = 42,000$ MW. A hydropower plant provides primary frequency control (FCR0) with $T_w = 1.2$ s, $T_g = 0.3$ s, $T_r = 5$ s and $g_{Tr} = 0.6$. The system was subjected to a disturbance of $\Delta P = 600$ MW. The droop is chosen such that the steady-state frequency deviation is 0.1 Hz, corresponding to a droop of 14% (gain of 7.1 pu/pu). The CL-base case was constructed as $T_{\text{base}} = G(s)/(1 + G(s)\text{FCR0}(s))$.

Next, an additional FCR reserve was added to the system in parallel with FCR0. The new FCR unit was also a hydropower plant with the same values of T_r, g_{Tr}, and T_w. Two cases were tested. In the first case, FCR1, we chose $T_g = 1.0$, which corresponds to a slow governor. In the second case, FCR2, we choose $T_g = 0.1$, which corresponds to a fast governor. We constructed CL systems as $T_{\text{FCR1}} = T_{\text{base}}/(1 + T_{\text{base}}\text{FCR1}(s))$ and $T_{\text{FCR2}} = T_{\text{base}}/(1 + T_{\text{base}}\text{FCR2}(s))$. We expect the slow governor to perform worse than the fast one.

6.2. Results

For the three CL models $T_{\text{base}}(s)$, $T_{\text{FCR1}}(s)$ and $T_{\text{FCR2}}(s)$, FDSI was used to identify the corresponding SOPZ transfer functions $\hat{T}_{\text{base}}(s)$, $\hat{T}_{\text{FCR1}}(s)$ and $\hat{T}_{\text{FCR2}}(s)$. The fit scores were 92.8, 89.4 and 89.6%, respectively. Figure 4 illustrates how SOPZ reduction simplifies the dynamics. The full model in Fig. 4(a) contains many poles and zeros, making it difficult to extract meaningful dynamical properties directly from the control-theoretic intuition. In contrast, the SOPZ approximation in Fig. 4(b) contains only two dominant poles and a single zero, from which the key properties can be directly inferred: $\omega_0 = |p|$, $\omega_d = \text{Im}(p)$, and the damping term $\zeta\omega_0 = -\text{Re}(p)$.

This reduction also enables a graphical comparison of how the additional reserves modify the system's performance. Both FCR1 and FCR2 move the dominant poles further from the real and imaginary axes, indicating improved damping and natural frequency. Moreover, FCR2 produced a larger horizontal pole displacement, which was consistent with its faster governor and the expectation that a faster unit contributes more damping to the system.

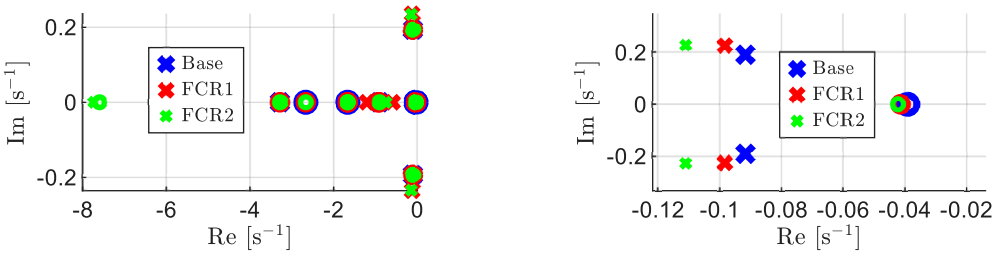

(a) (b)

Figure 4: Pole-zero plot of the systems. (a) Poles and zeros of without SOPZ approximation CL systems, $T(s)$. (b) poles and zeros of system with SOPZ approximations $\hat{T}(s)$.

The identified SOPZ parameters for each case are presented in Table 1. Table 2 further quantifies the contribution of each reserve by subtracting the base case values. As intended in the design of the case study, the reserve with the faster governor (FCR2) performed better. While ΔR_{tot} and $\Delta\omega_0$ are similar for both reserves, FCR2 achieves a larger reduction in τ_z (7.5% versus 5.6%) and, crucially, increases the damping ζ by 1.4%, whereas FCR1 reduces it by 7.7%. These results confirm that the SOPZ metrics capture the expected dynamic improvements associated with faster primary control.

Additionally, the SOPZ parameters allow the computation of the equivalent inertia H_{eq}, as listed in Table 3.

The step responses are shown in Fig. 5, which demonstrates that the

Case	R_{tot}	τ_z	ω_0	ζ
Base	0.142	25.587	0.212	0.433
FCR1	0.116	24.150	0.246	0.399
FCR2	0.115	23.669	0.253	0.439

Table 1: Parameters of the SOPZ model, expressed on standard form and as the equivalent system

Case	ΔR_{tot}	$\Delta\tau_z$	$\Delta\omega_0$	$\Delta\zeta$
FCR1	-0.025	-1.437	0.034	-0.033
	(-17.7 %)	(-5.6 %)	(16.2 %)	(-7.7 %)
FCR2	-0.027	-1.918	0.041	0.006
	(-19.0 %)	(-7.5 %)	(19.4 %)	(1.4 %)

Table 2: Quantification of how the additional reserves changes the system compared to the base case.

SOPZ approximations closely follow the full models across the entire time horizon, including a highly accurate prediction of the frequency nadirs. The zoomed view in Fig. 5(b) reveals the main limitation of this reduction: the SOPZ model initially predicts a slightly steeper decline in frequency. This corresponds to an overestimation of the initial $\text{RoCoF}_{\text{max}}$, which subsequently decreases after approximately 1s as the SOPZ model aligns with the numerical trajectory. This effect explains the underestimation of H_{eq} in Table 1.

Using the SOPZ parameters, we computed the estimated Δf_{max}, $\text{RoCoF}_{\text{max}}$, SSDF, and PM, as shown in Table 4. Table 5 lists the relative errors compared with the direct simulation. The frequency nadir was estimated with

Case	H_{eq}	reH_{eq} [%]
Base	3.076	-23
FCR1	2.933	-26
FCR2	2.878	-18

Table 3: Measured values of H_{eq} and relative error compared to the actul value $H = 4$ s.

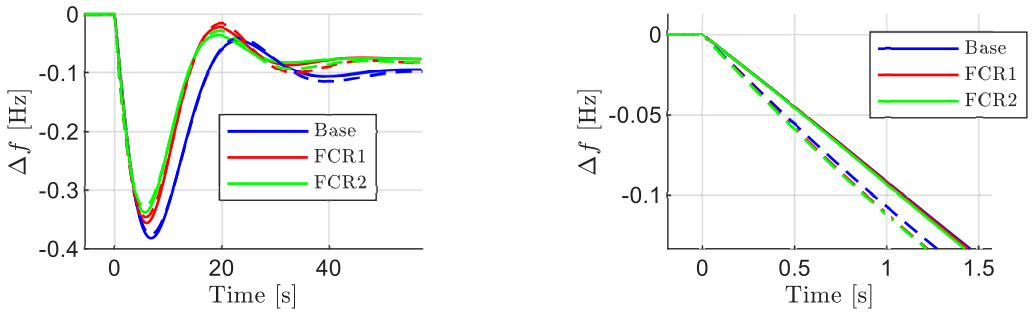

(a) (b)

Figure 5: Frequency response to a disturbance. The fully drawn lines were obtained from the simulation of the full system $T(s)$. Dashed lines are analytically calculated step responses of $\hat{T}(s)$.

high accuracy (within 3%), and the SSDF was within 10%. As expected from Fig. 5(b), the initial $\text{RoCoF}_{\text{max}}$ is overestimated by roughly 25–30%. The PM was correctly ranked between the cases, although the absolute error was larger owing to the infinite GM of the system.

6.3. Discussion

The case study demonstrated that the FDSI can identify an SOPZ model that accurately captures the essential frequency dynamics of the full system while substantially simplifying its structure. The SOPZ model reproduces

Case	$\Delta f_{\max}$ [Hz]	$\text{RoCoF}_{\max}$ [Hz/s]	SSFD	PM [deg]
Base	-0.375	0.116	0.101	23.514
FCR1	-0.346	0.122	0.083	31.186
FCR2	-0.329	0.124	0.082	37.413

Table 4: Estimation of Δf_{Max} and PM from SOPZ model.

Case	re $\Delta f_{\max}$[%]	re $\text{RoCoF}_{\max}$ [%]	re SSDF	re PM [%]
Base	1.7	24.1	-4.7	38.6
FCR1	2.8	28.8	-9.4	8.1
FCR2	2.8	29.2	-7.8	3.5

Table 5: fit score of FDSI and relative error of the estimations of Δf_{Max}, RoCoF, SSDF and PM from SOPZ model compared to numerical simulations.

the dominant behaviour of the step response and, in particular, provides an accurate estimate of the frequency nadir, which is often the most critical metric for evaluating automatic FCR performance.

The SOPZ parameters $(R_{\text{tot}}, \omega_0, \zeta, \tau_z)$ offer a transparent way to quantify how additional reserves modify system dynamics. Consistent with physical expectations, the faster governor (FCR2) provided a stronger stabilising contribution than FCR1. This is visible in the parameter changes, especially in ζ and τ_z, and in the pole movements in Fig. 4(b).

The main limitations arise from the estimation of the initial RoCoF and equivalent inertia. Because the FDSI weighting prioritises accuracy around ω_0, the SOPZ model does not fully capture the high-frequency behaviour that governs the instantaneous RoCoF. This leads to a systematic overestimation

of the maximum RoCoF and, correspondingly, an underestimation of H_{eq}. However, because the RoCoF of the SOPZ model aligned with the numerical model after approximately 1s, a more reliable inertia estimate could be obtained by evaluating the RoCoF at later times. This avoids the incorrect interpretation that additional services provide a physical inertia.

Overall, SOPZ reduction provides a useful and interpretable approximation for quantifying frequency dynamics and comparing the contributions of different reserves. While improvements are possible regarding the estimation of inertia and initial RoCoF, the method is sufficiently accurate for evaluating key system metrics, particularly the frequency nadir and damping-related properties of the system.

7. Conclusion

In this study, we present a technology-neutral method for quantifying the frequency dynamics of a power system and assessing the contribution of ancillary services to frequency control. Using frequency-domain system identification (FDSI), the closed-loop dynamics were reduced to a compact second-order model with one zero (SOPZ), which was characterised by four parameters that together captured the dominant behaviour of the system. Despite its simplicity, the SOPZ approximation reproduced the frequency-domain behaviour and time-domain step response of the full model with high accuracy, including an estimation of the frequency nadir within 3%. These results demonstrate that the essential dynamics governing frequency stability can be represented using only a few, interpretable parameters.

A proof-of-concept case study based on a reference hydropower unit showed

that the proposed method successfully distinguishes between reserves with different dynamic characteristics. The changes in τ_z, ω_0, and ζ consistently reflected the expected improvement from a faster governor, and the pole movements in the SOPZ model provided an intuitive visualisation of these effects. Although the method overestimated the initial RoCoF and consequently underestimated the equivalent inertia, these discrepancies were limited to the very early part of the response and did not affect the accurate reproduction of dominant dynamics.

Overall, the results indicate that the proposed approach provides a technology-neutral means of approximating and quantifying the frequency dynamics. This method offers a basis for systematically comparing diverse frequency control services and may support the development of performance-based procurement strategies for future low-inertia power systems. Future work may refine the estimation of high-frequency behaviour and apply the framework to a broader set of resources, including inverter-based and fast-acting services.

Declaration of AI-assisted technologies

During the preparation of this work, the author used Paperpal, Grammarly, and ChatGPT to help with spelling, grammar, and phrasing. After using these services, the author reviewed and edited the content as needed and took full responsibility for the content of the published article.

Funding

The author acknowledges the financial support of Svenska Kraftnät, the Swedish Energy Agency, and StandUp for Energy, which made this research

possible.

Declaration of competing interest

The authors declare that they have no financial interests or personal connections that might have influenced the work presented in this paper.

References

[1] U. Farooq, R. B. Bass, Frequency Event Detection and Mitigation in Power Systems: A Systematic Literature Review, IEEE Access 10 (2022) 61494–61519. doi:10.1109/ACCESS.2022.3180349.

[2] P. Kundur, Power System Stability and Control, EPRI Power System Engineering Series, McGraw-Hill, 1994.

[3] P. Tielens, D. Van Hertem, The relevance of inertia in power systems, Renewable and Sustainable Energy Reviews 55 (2016) 999–1009. doi:10.1016/j.rser.2015.11.016.

[4] F. Milano, F. Dörfler, G. Hug, D. J. Hill, G. Verbič, Foundations and Challenges of Low-Inertia Systems (Invited Paper), in: 2018 Power Systems Computation Conference (PSCC), 2018, pp. 1–25. doi:10.23919/PSCC.2018.8450880.

[5] B. K. Poolla, D. Groß, F. Dörfler, Placement and Implementation of Grid-Forming and Grid-Following Virtual Inertia and Fast Frequency Response, IEEE Transactions on Power Systems 34 (2019) 3035–3046. doi:10.1109/TPWRS.2019.2892290.

[6] Y. G. Rebours, D. S. Kirschen, M. Trotignon, S. Rossignol, A Survey of Frequency and Voltage Control Ancillary Services—Part I: Technical Features, IEEE Transactions on Power Systems 22 (2007) 350–357. URL: https://ieeexplore.ieee.org/document/4077135. doi:10.1109/TPWRS.2006.888963.

[7] L. Viola, S. Mohammadi, D. Dotta, M. R. Hesamzadeh, R. Baldick, D. Flynn, Ancillary services in power system transition toward a 100% non-fossil future: Market design challenges in the United States and Europe, Electric Power Systems Research 236 (2024) 110885. doi:10.1016/j.epsr.2024.110885.

[8] R. Eriksson, N. Modig, A. Westberg, FCR-N DESIGN OF REQUIREMENTS, Technical Report, ENTSO-E, 2017. URL: https://www.svk.se/contentassets/e5a38b7a16a443b290f5d49d42ea03c0/3---fcr-n-design-of-requirements.pdf.

[9] K. Das, M. Altin, A. D. Hansen, P. E. Sørensen, Inertia Dependent Droop Based Frequency Containment Process, Energies 12 (2019) 1648. URL: https://www.mdpi.com/1996-1073/12/9/1648. doi:10.3390/en12091648.

[10] K. G. S. Darshit S. Patel, A Low Order System Frequency Response Model for Large Power System and Adaptive Load Shedding, International Journal of Advanced Research in Electrical, Electronics and Instrumentation Engineering 04 (2015) 3845–3852. URL: http://ijareeie.com/upload/2015/may/8_A_Low.pdf. doi:10.15662/ijareeie.2015.0405008.

[11] L. Ljung, System Identification: Theory for the User, Prentice Hall Information and System Sciences Series, 2nd ed. ed., Prentice Hall, Upper Saddle River, N.J, 1999.

[12] Mathworks, Process Models - MATLAB & Simulink, 2025. URL: https://se.mathworks.com/help/ident/process-models.html, accessed 29 October 2025.